Reactive Molecular Dynamics with Material-Specific Coarse-Grained Potentials: Growth of Polystyrene Chains from Styrene Monomers

Karim Farah,* Hossein A. Karimi-Varzaneh, Florian Müller-Plathe, and Michael C. Böhm

Eduard-Zintl-Institut für Anorganische und Physikalische Chemie, Technische Universität Darmstadt, Petersenstrasse 20, D-64287 Darmstadt, Germany

Received: July 27, 2010; Revised Manuscript Received: September 15, 2010

We have developed a reactive molecular dynamics (RMD) scheme to simulate irreversible polymerization of realistic polymer systems in a coarse-grained resolution. We have studied the chain propagation of styrene to polystyrene. For monodisperse polystyrene samples, we reproduce the results of equilibrium MD simulations: density, end-to-end distance, radius of gyration, and different geometrical distribution functions. The RMD simulations on polydisperse systems should be considered as case studies intended to understand the influence of different tuning parameters of the RMD approach on calculated polymer quantities. The parameters for the irreversible polymerization include the number and position of the initiator units (I*) as well as capture radii r_I (r_P) defining the geometrical conditions for chain initiation (propagation) and a characteristic delay time τ_r separating two reactive MD time steps. As a function of the r_I (r_P) and τ_r, it is possible to model polymerization processes both in the limit of almost unrelaxed and fully relaxed samples. The strong influence of the spatial localization of the I* on the polymer size distribution is discussed in detail. The RMD results are used to formulate optimized computational conditions for the simulation of irreversible polymerizations, to explain observed trends in the polydispersity index, and to suggest experiments that might lead to an unexpected polymer size distribution.

1. Introduction

For quite a long time the development of connectivity-altering molecular dynamics (MD) and Monte Carlo (MC) methods had not been in the focus of computer simulation studies. The expected prohibitively long computer time demands of reactive MD (RMD) and MC (RMC) calculations seemed to be an obstacle for scientific activities in this direction. The increasing computational facilities in the past 15 years, however, initiated the development of reactive simulation techniques. The first RMD and RMC simulations aimed at generating equilibrated structures of chainlike and cross-linked polymers.[1−8] Khare et al. combined atomistic MD simulations with periodic MC trials to connect monomer units.[9] The approach of these authors as well as similar studies[1−8] has been performed with the intention to build up glassy structures. Successful RMD approaches on the basis of generic bead-and-spring models have been suggested by several groups to study the polymerization kinetics of linear chains as well as the structural properties of the resulting melts.[10−12] The efficient simulation method of Svaneborg et al. rendered possible the formation of topologically disordered polymer networks.[13] At roughly the same time, a first MC realization under consideration of translational, orientational, and reactive moves was published.[14] The end- and double-bridging MC algorithms of Theodorou et al. have grown into powerful methods for the generation of well-equilibrated polymer samples with chainlike or even more complex architectures.[15−18] In the approach of Liu et al., a dissipative particle dynamics has been used to study phase separation which is coupled with polymerization.[19]

In more recent contributions, new RMD and RMC methods have been suggested. A generic MD model using hard ellipsoids to map irreversible polymerization has been described by Correzzi et al.[20] An RMD scheme in a coarse-grained (CG) resolution to study the formation of polymer chains has been developed by Perez et al.[21] In addition to a Lennard-Jones interaction, these authors have coupled adjacent beads via the anharmonic finite extensible nonlinear elastic potential. In analogy to the RMD work of Akkermans et al.,[11] a capture radius had to be defined in the latter formalism to model reactive steps; see below. These reactive simulations[11,21] can be considered as an extension of the pioneering work of Gao.[10]

Outside the context of polymerization, RMD simulations on the basis of a local equilibrium have been described for very simple processes.[22−24] Smith et al.[25] have developed a RMD formalism to simulate the thermal decomposition of polymers and nanostructures. Similar processes have been studied by other groups.[26,27] Reactive force fields of quantum chemical accuracy, however, have not been combined yet with reactive MD or MC schemes in the study of polymerization processes.[28,29] Finally, we want to mention the reactive ensemble Monte Carlo method[30] developed to study the equilibrium behavior of reacting systems. On the basis of the existing RMD literature, the following picture appears. While simple local reactions in polymers can be modeled with system-specific force fields at an atomistic level, the majority of polymerization reactions have been described only at the CG level with generic potentials.[11,21]

It is the purpose of the present study to take new steps toward RMD simulations using CG potentials of specific systems. We have modeled the polymerization of styrene (parametrized and from here on denoted as ethylbenzene (EB)) to atactic polystyrene (PS). The CG mapping scheme employed is displayed in Figure 1. Each ethylbenzene monomer as well as each repeat unit of PS has been identified with a CG bead. The labels R

* To whom correspondence should be addressed. Tel: +49-6151-16-5289. Fax: +49-6151-16-6526. E-mail: k.farah@theo.chemie.tu-darmstadt.de.

10.1021/jp107001e © 2010 American Chemical Society
Published on Web 10/12/2010

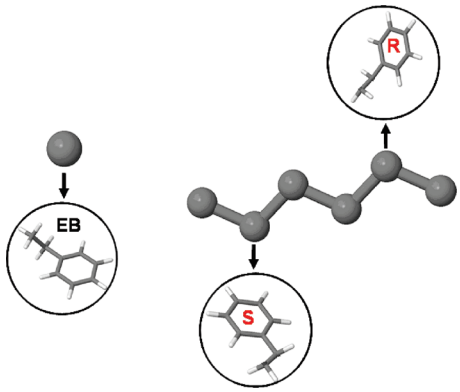

Figure 1. Coarse-grained mapping scheme for ethylbenzene (EB, left) as a model of styrene and for polystyrene (PS, right). A coarse-grained bead encompasses either one EB molecule ($(C_6H_5)C_2H_5$) or one repeat unit of PS ($-(C_6H_5)C_2H_3-$). In a PS chain, the two absolute configurations of the carbon center substituted by the phenyl rings give rise to CG beads symbolized by R and S. In atactic PS the sequence of the R and S beads is random.

and S in the schematic diagram characterize the two enantiomeric orientations of the −CHPh− group with Ph abbreviating a phenyl ring. The selection of CG polystyrene in our first RMD investigation is due to our recent simulation studies of this polymer.[31−34] A coarse-grained model for ethylbenzene and polystyrene as well as their mixtures has been tested in detail. Their temperature (T) transferability has been investigated in comprehensive equilibrium simulations.[31] In atomistic nonequilibrium calculations of PS and PS-CO_2 mixtures, we have analyzed the thermal conductivity of these species.[33,34] Crystalline syndiotactic PS has been chosen to study the correlation between the calculated thermal conductivity and degrees of freedom in a given force field.[32] The published CG potential of PS[31] adopted in the present article offers the possibility to compare RMD data for monodisperse PS samples with results of nonreactive equilibrium MD simulations on melts of a given chain length. Note that the CG potentials derived by Qian et al. were optimized to generate the same structure as the atomistic MD simulation. It should be noted that the present reactive MD implementation is an extension of the RMD model of Akkermans et al.[11] So far, the model has only been applied in connection with generic potentials which offer enough flexibility to simplify the implementation of a reactive MD scheme.[11,21] Employing specific potentials in RMD simulations is less straightforward as will be shown in the second and third sections. In contrast to former RMD studies, the focus is here more oriented on the growth history of the polymer samples. The present simulations show that qualitative features of polymerization experiments are already in reach.

The organization of the present paper is as follows. In the next section we explain the background of the developed RMD formalism. All simulations have been performed with the program IBIsCO which has been written in our group for CG studies of polymers.[35] The reactive MD extension of IBIsCO has led to the R-IBIsCO code. The computational conditions for the RMD calculations are given in the third section. In the fourth, we compare RMD results for monodisperse PS with the output of equilibrium simulations.[31] Before the conclusion, the growth history of the PS formation in polydisperse samples is related to experimental results in section 5.

2. Theoretical Background

The theoretical setup chosen allows the mapping of a so-called living polymerization with irreversible bond formation.[36,37] Before the polymerization of the monomers (M) can start (in the present work the polymerization of EB to PS), we have to define a certain number of monomer beads (N_I) which act as initiators (I*). Such an internal initiation occurs, e.g., in photopolymerizations. Each I* can bind one free monomer. In the succeeding polymerization steps, the terminal monomer (P*) of a polymer chain can react with a free monomer. Thus, the irreversible polymerization leads to the following reactive scheme, with the symbol * denoting a reactive unit:

$$\begin{aligned} &\mathrm{I}^* + \mathrm{M} \rightarrow \mathrm{I} - \mathrm{P}^* \\ &\mathrm{I} - \mathrm{P}^* + \mathrm{M} \rightarrow \mathrm{I} - \mathrm{P} - \mathrm{P}^* \\ &\mathrm{I} - \mathrm{P}_{n-1} - \mathrm{P}^* + \mathrm{M} \rightarrow \mathrm{I} - \mathrm{P}_n - \mathrm{P}^*,\ n = 2,3,4,... \end{aligned} \tag{1}$$

Suitable descriptors for such processes are the polymer size (degree of polymerization) N_L, its mean value $\langle N_L \rangle$, and the underlying distribution function $P(N_L)$ as well as the polydispersity index I_P. These quantities have been determined in the present reactive MD simulations. To emphasize this origin, in the following discussions they have been labeled with the index "sim". $\langle N_L \rangle_{sim}$ and I_{Psim} are defined as

$$\langle N_L \rangle_{sim} = \sum n_{N_L} N_L \tag{2}$$

$$I_{Psim} = \frac{N_w}{\langle N_L \rangle_{sim}} \quad \text{with} \quad N_w = \sum w_{N_L} N_L \tag{3}$$

The symbols n_{N_L} and w_{N_L} denote the number fraction and weight fraction.[38] The summations in relations (2) and (3) are performed over all possible values of N_L.

It has been mentioned in the Introduction that the present RMD implementation exhibits certain similarities with polymerization models suggested by Akkermans et al.[11] as well as Perez et al.[21] But in contrast to these generic schemes, we have employed a realistic CG potential derived for EB, PS, and EB-PS mixtures.[31] The present CG potential is defined by nonbonded interactions as well as by bonded radial and angle terms. These degrees of freedom are not considered in generic RMD schemes with potential functions that are not system-specific.

Reactive steps in the present RMD formalism are implemented as follows. We define two tuning parameters controlling the polymerization. The first is a characteristic delay time (τ_r) separating two succeeding time steps in which reactions are allowed to take place. The interval τ_r between such steps is reserved for normal MD without connectivity alteration, e.g., for the relaxation and diffusion of the particles. In order to simplify the implementation of the reactive processes, the parameter τ_r is kept constant during the simulations and is independent of the chain length. For small τ_r the particles do not have enough time to reach equilibrium via dynamic processes. RMD simulations under these conditions have been denoted as "static".[11,21] For large τ_r, the system has more time to relax and diffuse before new bonds can be formed. The time interval required for relaxation by molecular motions of course depends on the polymer weight fraction and the degree of polymerization. In contrast to the "static" processes in the limit of small τ_r, the descriptor "dynamic" has been employed in the RMD literature to classify simulations performed for large values of τ_r.[11,21] In the present RMD formalism the number of reactive time steps separated by τ_r is not limited. Each propagating chain as well as each initiator is allowed to form

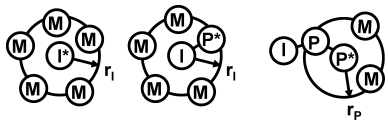

Figure 2. Schematic representation of the initiation step of the polymerization (left and center diagrams) as well as the chain propagation (right). The center diagram symbolizes the formation of a new I−P* bond. The two different reactive processes are characterized by capture radii r_I and r_P. The reaction can take place whenever a free monomer bead M comes into the interaction sphere r_I of an initiator I* or r_P of a terminal reactive chain monomer P*.

only one bond per reactive step. The maximum number of chains that can propagate simultaneously in a reactive step is equal to the initial number of starters N_I.

In addition to the delay time τ_r, we employ a geometric criterion compatible with bond formation at reactive time steps. This leads us to the second tunable parameter of our method. Bonding, at the allowed time steps, takes place whenever a free monomer is found in a sphere of radius r_I of an initiator bead I* or r_P of a terminal unit P* of a growing chain. If more than one free monomer lies within the capture radius of a reactive center, a bond is formed with the closest one. A schematic display for the reactive steps is shown in Figure 2. In the left (center) diagram characterizing the starting reaction the initiator can bind (has bound) a free EB monomer; in the right one a terminal monomer P* of the growing chain has formed a new bond (propagation).Whenever a new bond is formed, the CG potential, to be described below, switches instantaneously from a nonbonded interaction to a bonded one described by bond and angle terms. In contrast to the other reactive simulations employing such a geometric criterion,[11,21] we have used a force field where r_I (r_P) lies inside the repulsive part of the potential. The R-IBIsCO program written for the present research allows the definition of individual capture radii r_I (r_P) for the starting reaction and chain propagation. Thus, we can model different reactivities at the two topology-altering centers. For the reactive parameters r_I (r_P) as well as for the delay time τ_r, we had to choose values that lead to simulation times accessible with the present computational facilities. In our simulations, we have adopted capture radii between 0.55 and 0.40 nm. The nonbonded interactions at these r_I (r_P) values lead to energy barriers of 0.47 and 16.30 kJ/mol. They measure the difference between the minimum of the pairwise nonbonded potential and the energy derived at r_I (r_P). Modifications of this energy under the influence of the reactive process are not considered in our simple setup. Nevertheless, we suggest identifying these numbers in the context of the present RMD scheme as the activation energy E_A of the polymerization reaction. Note that these numbers are smaller than the E_A of living polymerizations. We expect, however, that qualitative aspects of the polymerization procedure can be reproduced by the present approach.

To sum up, in addition to the number N_I and position of the initiator beads I*, the present RMD scheme is controlled by two tuning parameters. The delay time τ_r separates two reactive MD steps where bond formations are possible. In principle, there is no limitation in the overall number of new bonds formed at reactive MD steps, as long as free monomers are available. Nevertheless, a reaction can only take place if the two reacting beads are located within a sphere of radius r_I (I−P* bonds) or r_P (P−P* bonds). The capture radii determine the activation energy for the polymerization. The delay time τ_r controls the degree of relaxation and diffusion between reactive MD steps; i.e., it is an element characteristic for the simulation method. Although of different physical meaning, the influence of r_I (r_P) and thus of E_A, on the one hand, and τ_r on the other hand, cannot be considered as completely independent. With the above choice of parameters, the present MD simulations have approximately the same time scale for the polymer dynamics and the chemical activation in the reactive steps. Although differing by many orders of magnitude in reality, they nevertheless allow the simulation of a living polymerization which provides insight on growth mechanisms. The introduction of the parameters N_I, r_I (r_P), and τ_r indicates that RMD simulations of polydisperse samples can be considered as a case study to test the sensitivity of the approach to these parameters. The present analysis of polydisperse samples, however, goes beyond the recent generic RMD simulations as it offers a qualitative access to experimental features; see the discussion in a later section.

We now come to the CG mapping of the chosen systems. We have employed an existing CG potential[31] derived via the iterative Boltzmann inversion (IBI) method, a highly stable algorithm developed by one of the present authors.[39] As target functions, Qian et al. made use of inter- and intramolecular distribution functions from atomistic simulations.[31] Atactic PS is characterized by a random arrangement of so-called R and S beads. The sequence of the two repeat units was determined by a random number generator with equal probabilities. There are two terms for the bonded "two-bead" interaction R-R (= S-S) and R-S (= S-R). The different types of angular potentials are symbolized by R-R-R (= S-S-S), R-R-S (= S-R-R = S-S-R = R-S-S), and R-S-R (= S-R-S). The nonbonded interactions are described by potential terms denoted R-R (= S-S) and R-S (= S-R). In analogy to nonreactive IBIsCO simulations, all potentials in R-IBIsCO are stored in tabulated form.

The correlation between RMD results for monodisperse PS and equilibrium data reported recently[31] is used as benchmark to estimate the capability of the present simulation scheme in generating equilibrated polymer structures. Even in conventional equilibrium MD calculations of complex systems, the possible trapping in quasi-degenerate configurations, which may differ in certain physical properties, requires a high computational effort.[40−42] A detailed discussion of such phenomena in non-equilibrium simulations of PS can be found in one of our recent articles.[33] It cannot be ruled out a priori that such problems are even enhanced in the presence of reactive processes. Thus, the comparison of RMD and equilibrium data can be considered as an additional test to recognize and, if necessary, to suppress the implications of such quasi-degeneracies.

3. Computational Conditions

All RMD simulations were performed in the constant-NPT ensemble where the particle number $N = N_M$ includes all beads in the system, i.e., the free monomer and initiator beads as well as the ones in the polymer chains. For simulations of monodisperse PS samples, we have chosen the temperature $T = 500$ K and the pressure $P = 101.3$ kPa to meet the conditions of the equilibrium runs which served as reference.[31] The total number of CG beads adopted in the benchmark studies amounts to $N_M = 3840$. Monodisperse samples have been generated with the help of a predefined chain length N_L. If a growing chain has reached this limit, further reactive processes are forbidden by definition. At the end of the simulation we have N_I polymer chains with identical length N_L. A complete list of the parameters defining the present RMD approach can be found in Table 1. For the monodisperse simulations, the initial number of initiators is determined by the ratio $N_I = N_M/N_L$ with $N_L = 10$, 30, 80, and 120. In a first stage, growth and equilibration of the monodisperse samples are performed until all free monomers

TABLE 1: Summary of Input Parameters and Quantities Used in the Present RMD Simulations of a Living Polymerization

N_M	total number of monomer beads including the initiators I*
$N_I = N_P$	total number of initiators N_I which coincides with the total number of chains N_P
N_{Ir}	number of initiators that have reacted at a certain polymerization time
N_L	degree of polymerization of a polymer chain
D_P	conversion (percentage of monomers converted into polymer beads)
r_I (r_P)	capture radius of the initiator I* (terminal monomer bead P* of a chain)
I_P	polydispersity index
N_G	total number of growth steps, i.e., number of reactive MD steps
τ_r	time interval (in ns) between two reactive MD steps
$t_{1/2}$	time to reach a 50% conversion of the free monomers M into polymer beads P
t_∞	time to complete the polymerization $D_P(t_\infty) = 100\%$

have been captured. The values of the capture radius and delay time adopted here are $r_I = r_P = 0.40$ nm and $\tau_r = 5 \times 10^{-4}$ ns. Long equilibration runs are subsequently performed for these monodisperse samples. Following the equilibration the quantities of interest are extracted from the samples.

In the simulation of polydisperse samples, the constraint of a common N_L is simply removed. These calculations have been performed at $P = 101.3$ kPa and $T = 400$ K which is a characteristic condition for the living polymerization of styrene to PS.[43,44] To derive the CG potential for this temperature, we have used the temperature-dependent scaling factor of ref 31, $f(T) = (T/T_0)^{1/2}$ where $T_0 = 500$ K is the temperature for the development of the CG force field. The CG potential at $T = 400$ K requires a simple transformation of the potential by the multiplicative factor $f(T) \approx 0.894$. A qualitative justification of the square-root dependence of the factor $f(T)$ can be found in ref 31. The polydisperse samples have been modeled by considering $N_M = 4000$ including an initiator number N_I of 80 beads. The chosen N_M/N_I ratio is quite close to the relative concentrations of the components in experiments.[43,44] All reactive MD simulations (monodisperse and polydisperse samples) have been continued until the last free monomer had been captured by one of the growing chains.

Constant time steps of 5 fs have been employed in the reactive simulations. The Berendsen thermostat[45] is used with a coupling time of 0.5 ps, while a coupling time of 5 ps has been chosen for the barostat. These time constants are combined with an isothermal compressibility of 1×10^{-6} kPa^{-1}. The cutoff for the nonbonded interactions has been set to 1.6 nm, and the associated Verlet neighbor list cutoff value is 1.7 nm. The updating procedure for the neighbor list has to be at least equal to the delay time τ_r to monitor the time evolution of the system topology correctly. The values for the capture radius r_I (r_P) and the delay time τ_r employed in the different RMD simulations are quoted in sections 4 and 5.

The alteration of the particle connectivity requires a permanent control of the system. Whenever a new bond is formed, the interaction potential between the reacting beads is switched instantaneously from a nonbonded to a bonded interaction. The implications of this process for the entries in the neighbor list are evident: the RMD code has to guarantee that the newly connected beads do not feel nonbonded interactions up to the second neighbors in the chain. All simulations have been performed under periodic boundary conditions and the minimum image convention.

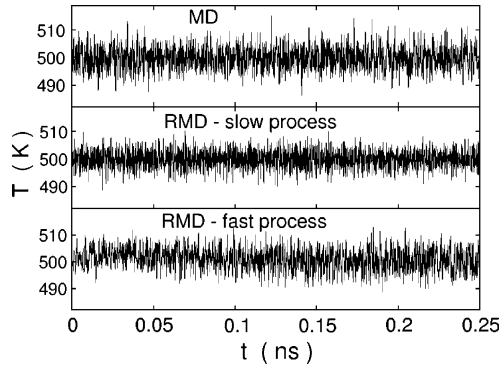

Figure 3. Temperature fluctuations as a function of the simulation time t. The top diagram represents the T dependence of a conventional equilibrium MD simulation of a monodisperse sample with $N_L = 80$. The T fluctuations in the other diagrams refer to reactive MD simulations. Center plot: $D_P = 30\%$, $r_I = r_P = 0.40$ nm, $\tau_r = 5 \times 10^{-4}$ ns. Bottom plot: $D_P = 90\%$, $r_I = r_P = 0.55$ nm, $\tau_r = 5 \times 10^{-4}$ ns. The target temperature is $T = 500$ K.

At the end of this section we analyze the stability of the present RMD implementation. We just have emphasized that each reactive event between two beads is accompanied by a spontaneous switch of the CG potential from a nonbonded to a bonded interaction. In Figure 3 we show that the excess heat produced in these processes does not lead to significant changes in the temperature fluctuations. The target temperature adopted in these reactive MD runs is 500 K. The top diagram provides the T fluctuations in a conventional equilibrium simulation (i.e., absence of reactive processes). In the middle diagram we have plotted the temperature fluctuations in a polydisperse sample at a conversion of 30%. The RMD runs are performed with $r_I = r_P = 0.40$ nm and $\tau_r = 5 \times 10^{-4}$ ns; i.e., we follow a slow process. It can be seen that the formation of new bonds does not lead to any increase of the temperature. The same behavior is found when increasing the conversion continuously, i.e., in the limit of complete polymerization. In the faster process shown in the bottom diagram ($r_I = r_P = 0.55$ nm and $\tau_r = 5 \times 10^{-4}$ ns), only a slight increase of T of roughly 2 K near the time origin can be detected. This increase is due to the switching from the nonbonded to the bonded potentials when bonds are being formed in this fast process. But even this excess energy is quickly removed from the system by the Berendsen thermostat with standard settings. In analogy to the middle diagram, the bottom T profile is characteristic for the whole reactive process. Finally, we also have checked the length fluctuations of a bond formed at a certain time $t = 0$ up to the end of the reactive simulation (results not shown here). The length fluctuations of the bonds formed during the reactive simulations are similar to those experienced by the same system simulated with standard MD (i.e., topology of the system fixed at the beginning of the simulation).

4. Growth of Monodisperse Systems: Validation of the Method

We have chosen the density (ρ) as the first quantity to present the correlation between equilibrium MD and RMD data for monodisperse PS samples. All nonreactive equilibrium simulations reported below have been repeated for the present work by adopting the setup described by Qian et al.[31] In the top diagram of Figure 4 we have plotted the density of PS as a function of the predefined chain length N_L. The agreement between MD and RMD data is very good. The equilibrium MD and RMD densities for $N_L = 10$, 30, 80, and 120 differ by less

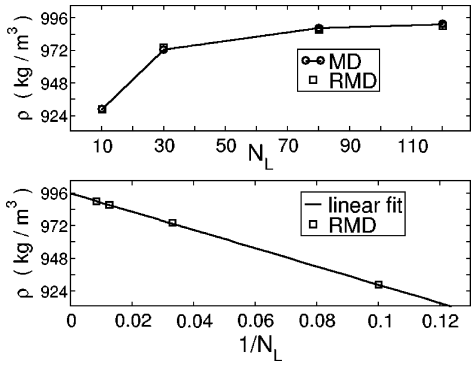

Figure 4. Density ρ of monodisperse polystyrene samples as a function of the predefined chain length N_L (top diagram) and as a function of $1/N_L$ (bottom diagram). The data points of the standard equilibrium MD simulations (circles) in the top diagram have been connected by a full line as a guide to the eye, the reactive MD (RMD) derived data are represented by squares. The bottom diagram shows the RMD data (squares) along with the fitted linear curve used for an extrapolation of the density of a monodisperse system with an average chain length of 500 monomers.

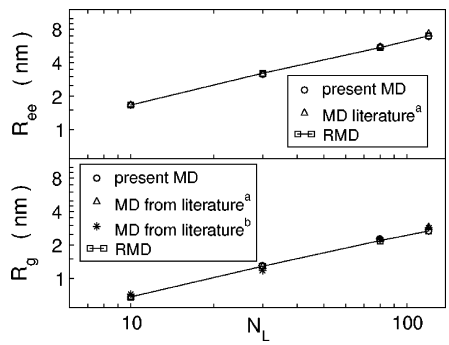

Figure 5. Root-mean-square end-to-end distance R_{ee} (top) and radius of gyration R_g (bottom) for monodisperse PS of chain lengths N_L = 10, 30, 80, and 120 as derived by standard and reactive MD simulations. All simulations have been performed at T = 500 K. Note the double logarithmic representation of the plot. The literature data labeled by "a" and "b" have been taken from refs 31 and 48, respectively.

than 1%. The 500 K density of the initial EB sample amounts to 631.1 kg/m^3. With increasing length of the polymer the density increases. The present MD and RMD densities are of the same order of magnitude as experimentally determined values. In ref 46, a density of 950 kg/m^3 at T = 500 K has been reported for atactic PS. It refers to a polymer sample with an average molecular weight of 51 000 g/mol corresponding to an averaged chain length of 500. The bottom diagram of Figure 4 contains the RMD based densities as a function of the inverse polymer size N_L. In this linear correlation, the limit $1/N_L \rightarrow 0$ can be used to estimate the density of polymers with long chains. For N_L = 500 the extrapolation leads to a density of 995 kg/m^3 which differs by less than 5% from the experimental value.

The same good agreement between equilibrium and RMD results for PS is observed for the root-mean-square end-to-end distance $R_{ee} = \langle R_E^2 \rangle^{1/2}$ and gyration radius $R_g = \langle R_G^2 \rangle^{1/2}$. R_E (R_G) symbolizes the end-to-end distance (radius of gyration). The N_L dependence of R_{ee} is shown in Figure 5 (top diagram) along with the simulation results of Qian et al.[31] The RMD-based scaling exponent v in the relation $R_{ee} \propto N_L^v$ of 0.571 differs by less than 3% from the theoretical estimate for self-avoiding walks of v = 0.588. This value of v is characteristic for the excluded volume behavior of short chains.[11,47] For the radius of gyration (Figure 5, bottom diagram) we have correlated the present RMD and MD results with two equilibrium

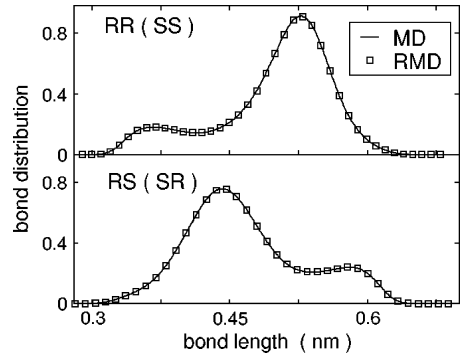

Figure 6. Bond length distribution between the centers of mass of RR (SS) and RS (SR) beads in atactic polystyrene (top, bottom) from the present RMD approach and a conventional equilibrium MD simulation. The data refer to N_L = 120 and T = 500 K.

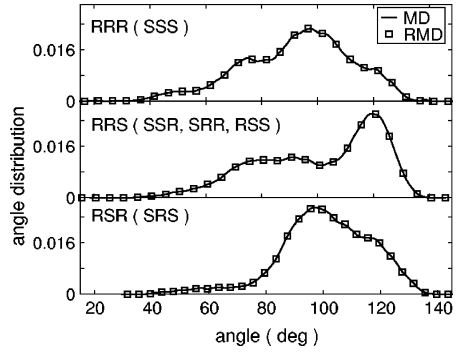

Figure 7. Angle distribution between three adjacent repeat units of atactic PS from the present RMD approach and in standard equilibrium MD simulations. The data refer to N_L = 120 and T = 500 K.

simulations from the literature.[31,48] As expected on the basis of the R_{ee} plot, we again observe a linear relation between R_g and N_L when plotted in a double-logarithmic scale. All equilibrium results considered in the benchmark studies are reproduced perfectly by the reactive MD approach. Thus, it seems that sampling problems[40,41] are small for the quantities derived for monodisperse PS samples by the two different MD techniques.

We continue our comparative analysis of monodisperse PS in CG resolution with distribution functions for the bonds and angles. In Figure 6 we show the length distribution between the centers of mass of bonded beads as derived under RMD and conventional equilibrium MD conditions. The same comparison between the two computational schemes for the angle distributions of the bonded beads is reported in Figure 7. The curves in both figures have been evaluated for a predefined chain length N_L of 120 beads. Again, we notice an excellent agreement between the connectivity-altering and the equilibrium MD runs. The same is valid for the angle distributions in Figure 7. From Figures 6 and 7, we deduce that intramolecular length and angle distributions are correctly determined by the present RMD method. The same agreement between the two MD codes has been observed for the other chain lengths studied (N_L = 10, 30, 80). The intramolecular distributions plotted in Figures 6 and 7 confirm the trends already formulated in connection with the density as well as the R_{ee} and R_g profiles.

A comparison of the nonbonded radial distribution function $g(r)$ between RR (SS) beads for monodisperse PS chains with N_L = 120 and 10 concludes our validation of the RMD implementation. In analogy to the bonded distribution curves, also the nonbonded ones in Figure 8 are correctly reproduced by the RMD method. Thus, the present connectivity altering MD code is an efficient tool to derive equilibrated structures of

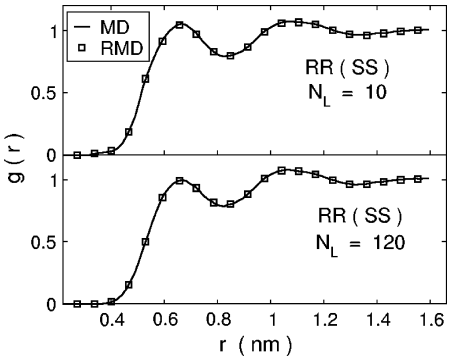

Figure 8. Nonbonded radial distribution functions $g(r)$ between RR (SS) beads of atactic PS with $N_L = 10$ (top) and $N_L = 120$ (bottom) from the present RMD approach and conventional equilibrium MD simulation at $T = 500$ K.

TABLE 2: Characteristic Times (Half-Life $t_{1/2}$ and Time to Full Conversion t_∞) as a Function of the Capture Radius $r = r_I = r_P$ in RMD Simulations of Polydisperse Samples[a]

$r_I = r_P$	$t_{1/2}$	t_∞
0.40	6.00	29.6
0.45	0.40	2.5
0.48	0.13	1.2
0.55	0.03	0.86

[a] The delay time is $\tau_r = 5 \times 10^{-4}$ ns. The values $t_{1/2}$ and t_∞ are given in ns and r_I and r_P in nm.

monodisperse polymer samples. On the basis of the above simulation results, we strongly feel that the RMD approach should be also a useful tool to study the properties of polydisperse systems under different growth conditions.

5. Growth History in Polydisperse Samples

The polymer growth in the monodisperse samples of the last section has been terminated by the predefined parameter N_L which defines the common length of all chains. In the simulations described below, this constraint on N_L has been removed in order to allow a free growth of the N_I different polymer chains. In analogy to monodisperse samples, we have again a good agreement between the calculated ρ of 1025 kg/m^3 and measured values of 1005 and 1013 kg/m^3. The experimental data refer to samples with an averaged chain length of 500 monomers,[46,49] while the RMD results correspond to a value of roughly 50 at $T = 400$ K. The literature data have been recorded at $T = 408$ K.

A. Influence of the Capture Radius and Delay Time. In this section, the initiator positions have been distributed randomly in the simulation box. First, we have chosen a common capture radius r ($r = r_I = r_P$) for the initiator I* and the terminal polymer bead P* in the chains at a constant value of the delay time $\tau_r = 5 \times 10^{-4}$ ns. Numerical results on the correlation between r and characteristic polymerization times are given in Table 2 where we have collected the parameters $t_{1/2}$ and t_∞ as a function of r. The time $t_{1/2}$ indicates that one-half of the initial free monomers M has been converted into polymer beads P (i.e., $D_P = 50\%$), while t_∞ denotes that the polymerization process has been completed (i.e., $D_P = 100\%$). The $t_{1/2}$ numbers indicate that an increase of r from 0.40 to 0.55 nm leads to an enhancement of the reaction velocity by a factor of 200. This acceleration is a manifestation of the higher probability to find a monomer in the vicinity of a terminal chain bead if the capture radius is enlarged. This can be quantified by averaging the number of free beads within the capture radius

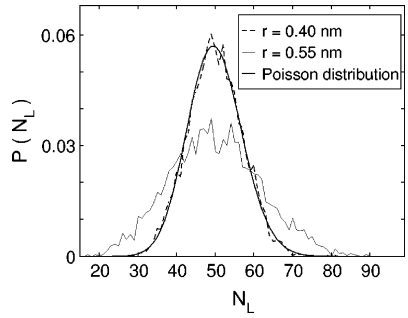

Figure 9. Distribution function $P(N_L)$ for the polymer size N_L from RMD simulations with $r = 0.40$ nm and with $r = 0.55$ nm ($r = r_I = r_P$). The value of the delay time is $\tau_r = 5 \times 10^{-4}$ ns. Both RMD curves have been averaged over 55 simulations. Each simulation starts with a different random initial distribution of the starters in the box. The bold curve is a Poisson profile (analytical solution (4)) derived by assuming that all polymerization steps can be described by the same rate law and rate constant.

of a reactive bead during a certain simulation time. For $r = 0.55$ nm the averaged number of free beads in the reactive sphere of the chain end during 0.03 ns is 0.63. Note that 0.03 ns refers to the time to reach $D_P = 50\%$. For the same time of simulation (i.e., 0.03 ns) the averaged number of free beads found within a capture radius of 0.40 nm is reduced to 0.0125. In contrast to $t_{1/2}$, the time to full conversion t_∞, however, differs by only a factor of roughly 34. This leveling indicates the decelerating influence of equilibration and diffusion steps in the end phase of a polymerization even if these factors are unimportant at the beginning of a fast reaction.

We come to the influence of r on the degree of polymerization N_L of the N_I polymer chains. The final chain length distribution $P(N_L)$ derived for $\tau_r = 5 \times 10^{-4}$ ns has been plotted in Figure 9 for the two limiting r considered (0.40 and 0.55 nm). The fast reaction (large r) leads to a broader $P(N_L)$ profile.

The small activation energy associated to $r = 0.55$ nm allows reactive steps in configurations only partially relaxed that are characterized by a trapping of initiator units or terminal polymer beads in a nonreactive surrounding.

Under certain assumptions, it is possible to solve the kinetic equations for a polymerization process analytically. In this framework, it is assumed that the reaction rate coefficient for the bimolecular reaction (I-P$_{n-1}$-P* + M) is independent of N_L. This is fulfilled under the following conditions. (i) The reactants have to be ideally mixed preventing a diffusion control. (ii) The initiation kinetics has to be fast relative to the chain propagation. Condition (ii) will be examined in more detail in following subsections. The analytical solution for $P(N_L + 1)$ corresponds to the following Poisson distribution function.

$$P(N_L + 1) = \frac{N(t)^{N_L}}{N_L!} \exp[(-N(t))] \quad N_L = 1,2,... \quad (4)$$

$N(t)$ is the average number of bonds per chain (ratio between the total number of bonds formed and the total number of activated chains) at any time t. The recurrence formula offers an access to the fraction of polymers with polymerization degree $N_L + 1$ (number of polymer chains with length $N_L + 1$ divided by the total number of growing chains). In addition to the two RMD curves in Figure 9, we have displayed the $P(N_L)$ profile using the above Poisson formula. For more information we refer to the literature.[11] Figure 9 indicates that the $r = 0.40$ nm simulations follow a Poisson-like behavior. Thus, we can

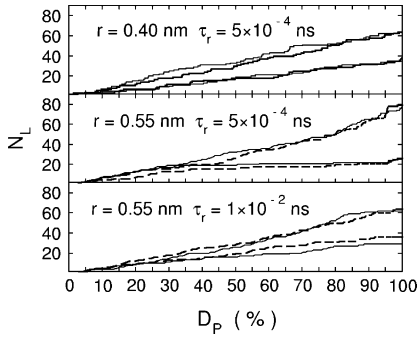

Figure 10. Evolution of the polymer size N_L for the two shortest and the two longest chains as a function of the conversion D_P in RMD simulations performed with $r = 0.40$ nm (top) and $r = 0.55$ nm (middle) associated with $\tau_r = 5 \times 10^{-4}$ ns. The bottom diagram has been evaluated with $r = 0.55$ nm and $\tau_r = 1 \times 10^{-2}$ ns.

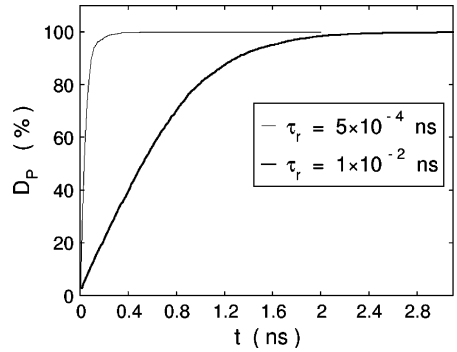

Figure 11. Time dependence of the conversion D_P (%) for $\tau_r = 5 \times 10^{-4}$ ns (thin curve) and 1×10^{-2} ns (bold curve). Both RMD curves use $r = 0.55$ nm for all reactive centers.

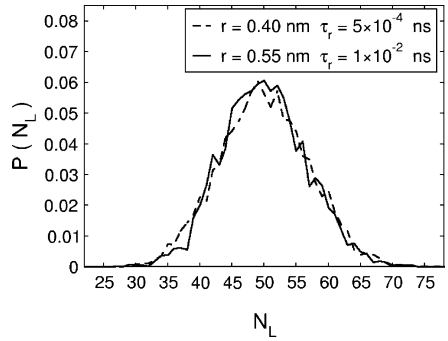

Figure 12. Distribution $P(N_L)$ of the polymer size N_L on the basis of two different (r,τ_r) combinations. The full curve corresponds to $r = 0.55$ nm, $\tau_r = 1 \times 10^{-2}$ ns, and the broken one to the combination $r = 0.40$ nm, $\tau_r = 5 \times 10^{-4}$ ns.

conclude that equilibration and diffusion seem to be fast compared to the polymerization rate with this small r value. In the $r = 0.55$ nm case, the deviation of the $P(N_L)$ profile from the Poisson-like behavior is due to trapping effects as described in the following paragraph.

To emphasize differences in the growth history of the polymers as a function of r, we have calculated the length N_L for the two longest and shortest chains as a function of the conversion D_P. The curves in the top and middle diagrams of Figure 10 refer again to the limiting capture radii r of 0.40 and 0.55 nm combined with $\tau_r = 5 \times 10^{-4}$ ns. The bottom diagram of Figure 10 will be considered later in this subsection. It appears from the top and center diagrams that up to $D_P \approx 30\%$ there is no large difference in the growth history of the fast and slow polymerization. For $D_P > 30\%$ trapping processes appear in the simulation with $r = 0.55$ nm and $\tau_r = 5 \times 10^{-4}$ ns. They cause a split between the N_L profiles of the short and long chains which increases as polymerization proceeds. The implications of such processes in the presence of a small energy barrier have been visualized already in Figure 9.

For the polymerization simulated with $r = 0.55$ nm and $\tau_r = 5 \times 10^{-4}$ ns, eq 3 leads to a polydispersity index I_{Psim} of 1.058. The relaxation and diffusion processes allowed under $r = 0.40$ nm imply a small reduction of I_{Psim} to 1.020. These polydispersity indices are the results of an average over 55 RMD simulations for each of these two cases. Considering the differences in the chain lengths of experimental systems and the present simulations, the splitting between the calculated I_{Psim} and experimental numbers of roughly 1.3 for living polymerization is not unexpected.[21] Nevertheless, we feel that the calculated I_{Psim} numbers emphasize that the present RMD simulations of a living polymerization in a CG resolution offer a reliable description of the kinetics. By means of the local reaction parameter r it has been possible to simulate a transition from a "static" polymerization (r large, τ_r small) to a "dynamic" scheme (r and τ_r small). From the simulations it appears that $r = 0.40$ nm ($E_A = 16.3$ kJ/mol) seems to be sufficient for a proper consideration of equilibration and diffusion processes in the sample of growing polymer chains.

In order to investigate the influence of the delay time, we have adopted two different τ_r values of 5×10^{-4} and 1×10^{-2} ns with a constant capture radius $r = 0.55$ nm. In Figure 11 we have plotted the conversion as a function of the simulation time. Of course, the polymerization is faster when using the smaller τ_r value of 5×10^{-4} ns. Here the polymerization is finished after 0.86 ns while t_∞ in the $\tau_r = 1 \times 10^{-2}$ ns equals 3.20 ns. In analogy to the r-dependent simulations, let us now follow the growth history of the two longest and shortest PS chains as a function of τ_r. The curves in the bottom diagram of Figure 10 have been derived for $r = 0.55$ nm and $\tau_r = 1 \times 10^{-2}$ ns. The results of this diagram are compared to the evolution of the curves in the middle diagram derived with the same capture radius r but a smaller τ_r. As could be expected on the basis of the above findings, trapping effects are more or less absent in the "dynamic" simulation with $\tau_r = 1 \times 10^{-2}$ ns.

The RMD results presented up to now suggest, as expected, that r and τ_r cannot be considered as completely independent control parameters. This means that similar growth histories of the polymer chains can be modeled by different combinations of the delay time between reactive steps τ_r and the capture radius r. This computational degree of freedom can be extracted from Figure 12 where we have plotted the probability function $P(N_L)$ for two (r,τ_r) combinations: (0.55 nm, 1×10^{-2} ns) and (0.40 nm, 5×10^{-4} ns). Both reactive MD runs lead to almost identical $P(N_L)$ profiles. The advantage of this one-to-one mapping under different simulation conditions is evident. In fact, the simulation with (0.55 nm, 1×10^{-2} ns) is approximately 10 times faster.

B. Influence of the Spatial Distribution of the Initiator Beads. All RMD simulations discussed up to now have been performed for samples with a random distribution of the initiator beads I*. Now we relate these data to RMD runs starting from a spatially localized distribution of the I*. Experimentally, such an arrangement can be generated by a local photoinitiation or by the proper arrangement of the entrance slots for the initiators in the reactor. From technical polymerizations it is known that the size of the reaction vessel, its geometry, and the velocity of the component mixing can have a strong influence on the chain lengths and polydispersity index.[36] By changing the localization of the initiators I* in the simulation box, a case study for such

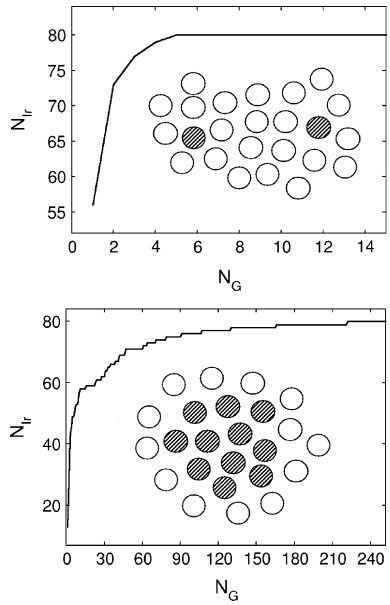

Figure 13. Number of initiators that have reacted N_{Ir} as a function of the number of reactive steps N_G. The top curve has been derived for a random distribution of the initiators, while the bottom one refers to a spatially localized initial configuration of the initiators. Both RMD simulations have been performed with $r = 0.55$ nm and $\tau_r = 5 \times 10^{-4}$ ns.

an experimental control element can be performed. A localized concentration of the I* is generated as follows. Before starting the RMD run, one EB bead is randomly chosen as initiator I*. The remaining members of the initiator ensemble are then selected on the basis of a simple cutoff criterion (i.e., the 79 beads closest to the chosen starter serve as the remaining I*).

Let us first consider the influence of the localization of the initiator beads on the number of I* forming an I−P* bond (N_{Ir}) as a function of the number of reactive MD steps (N_G). In Figure 13 we have plotted such curves for a random and a spatially localized distribution of the 80 initiators. The RMD results have been derived for $\tau_r = 5 \times 10^{-4}$ ns and $r = 0.55$ nm. From the figure we see that only $N_G = 5$ reactive MD time steps are required in the sample with randomly distributed I* to allow the 80 initiators I* to bind a monomer. $N_G = 5$ corresponds to a simulation time of 25 fs. The spatially localized I* distribution needs roughly 220 reactive steps to generate 80 growing chains. The simulation time associated to $N_G = 220$ amounts to 1100 fs. The different behavior between the two consumption curves of I* is easy to explain. For the localized I* arrangement, only the I* at the surface of the initiator droplet can find a reactive partner; the inner ones are trapped. Possible trapping effects as a function of the reactive parameters r and τ_r have been commented on above. From the discussion of the growth history of the chains under the influence of these parameters (previous section), we expect that trapping leads to broadened polymer size distributions. This is confirmed by the $P(N_L)$ curves in Figure 14. They are based either on $\tau_r = 5 \times 10^{-4}$ ns (top) or on 1×10^{-2} ns (bottom). The $P(N_L)$ profiles have been derived for the two extremal I* distributions considered (random and localized arrangements). The $\tau_r = 5 \times 10^{-4}$ ns polymerization with the smaller time interval for relaxation and diffusion between the reactive steps leads to large differences between the two $P(N_L)$profiles. The nonreactive surrounding of the inner I* in the droplet is responsible for an extremely broad $P(N_L)$ curve with two maxima. The first one occurs for N_L slightly below 10. It indicates that, as expected, some of the initiator

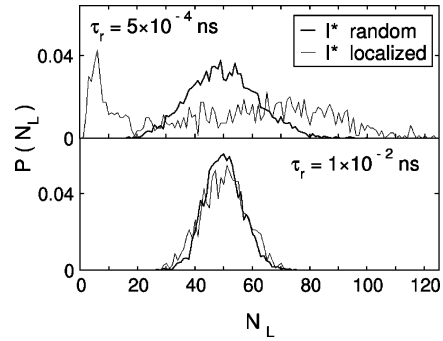

Figure 14. Distribution $P(N_L)$ of the polymer size N_L calculated with a random (bold curves) and a spatially localized (thin curves) distribution of the initiator beads I*. The curves in the top diagram are based on $\tau_r = 5 \times 10^{-4}$ ns, the curves in the bottom one on $\tau_r = 1 \times 10^{-2}$ ns. All simulations have been performed with $r = 0.55$ nm.

beads have been captured in a nonreactive surrounding for a rather long time. The second $P(N_L)$ maximum in the curve derived for localized I* appears at $P(N_L) \approx 70$. The double-peak structure of the $P(N_L)$ profile obtained for the spatially localized I* reflects that the trapping of some I* enables the growth of long polymer chains in the subset of untrapped reactive polymer ends.

From Figure 14 we deduce that a spatial localization of initiator beads can lead to a length or mass profile of the chains strongly different from the Poisson-like distribution shown above. A Poisson-like profile occurs under conditions where relaxation and diffusion in the sample are fast in comparison to the chain propagation. The double-peak curve in Figure 14 can be considered as an extreme example where this balance is violated. It remains an open question whether such a mass distribution could be obtained in an experiment. We are aware that the polymerization dynamics modeled by the present RMD approach is much faster than any experimental one. But if there was a chance to achieve this limit, two conditions would have to be fulfilled. The activation energy has to be very low and high sample viscosities would help to decelerate relaxation and diffusion. The lower diagram in Figure 14 emphasizes that the difference between the two $P(N_L)$ profiles disappears when performing the RMD runs under "dynamic" conditions ($\tau_r = 1 \times 10^{-2}$ ns). Both curves are quite similar and have their maximum at $N_L \approx 50$. The longer delay time τ_r between reactive MD steps allows the I* to spread into reactive domains of the sample before chain elongation under nonequilibrium conditions takes place.

In analogy to the forgoing calculations, the simulations starting from spatially localized initiators should provide insight into conditions supporting trapping. Figure 15 contains the length of the two shortest chains obtained under $\tau_r = 5 \times 10^{-4}$ ns (bold curves) and $\tau_r = 1 \times 10^{-2}$ ns (thin curves). Trapping is almost absent under "dynamic" conditions compatible with $\tau_r = 1 \times 10^{-2}$ ns. Here even the shortest chains contain more than 30 monomers. The N_L increase continuously with increasing polymerization. The reduction of τ_r from 1×10^{-2} to 5×10^{-4} ns is responsible for an almost perfect trapping of the reactive terminal beads of the chains. At the end of the polymerization, chains with only three or five monomers are left. We believe that Figures 14 and 15 provide useful information on the implications of localized initiator concentrations in living polymerizations.

C. Different Capture Radii for the Initiation and Chain Propagation. We now relate polymerizations performed under $r_I = r_P$ to $r_I \neq r_P$ ones; i.e., we consider different activation

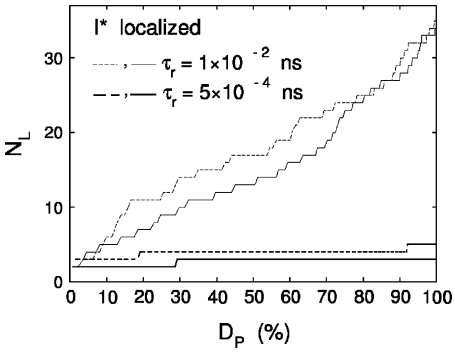

Figure 15. Evolution of the size N_L of the two shortest chains in RMD simulations starting from a localized initiator concentration for $\tau_r = 5 \times 10^{-4}$ ns and $\tau_r = 1 \times 10^{-2}$ ns. All simulations employ $r = 0.55$ nm.

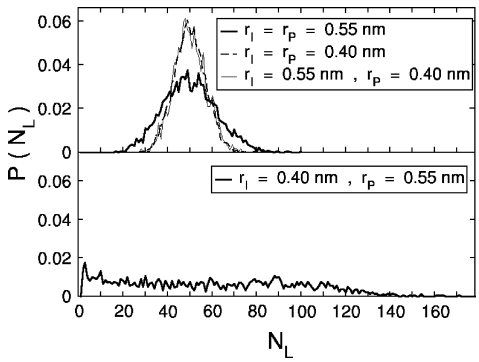

Figure 16. Distribution $P(N_L)$ of the polymer size N_L for a RMD run with $r_I = 0.55$ nm and $r_P = 0.40$ nm as well as for two homogeneous processes with $r_I = r_P = 0.40$ and 0.55 nm (top diagram). The $P(N_L)$ distribution in the bottom diagram has been evaluated for $r_I = 0.40$ nm and $r_P = 0.55$ nm. All simulations have been performed with a delay time τ_r of 5×10^{-4} ns.

energies for the reaction of the initiator I* with a monomer and the chain propagation. In this section, the term "homogeneous" is used to denote simulations performed with $r = r_I = r_P$. In polymerization reactions, one usually has lower activation energies for the initiation step than for the propagation.[37] With the present RMD model, this can be mapped by setting $r_I > r_P$. Let us go to the top diagram of Figure 16 where we have plotted the probability $P(N_L)$ of a process modeled by $r_I = 0.55$ nm and $r_P = 0.40$ nm together with two homogeneous profiles evaluated for common radii ($r_I = r_P$) of either 0.55 or 0.40 nm. All RMD results have been obtained for $\tau_r = 5 \times 10^{-4}$ ns. The simulations show that the energy demand for the starting reaction is without influence on the size distribution and polydispersity index if the chain propagation requires a higher or equal activation energy. The $r_I \neq r_P$ curve and the homogeneous one with high activation energy are similar; both reproduce a Poisson-like behavior. The reasons leading to the broad $P(N_L)$ for the homogeneous runs with $r_I = r_P = 0.55$ nm have been commented on in the foregoing discussion.

The time demand for the formation of 80 growing polymer chains for simulations with $r_I = 0.55$ nm and $r_P = 0.40$ nm differs from the ones with $r_I = r_P = 0.40$ nm. In the RMD study with $r_I = 0.55$ nm, only five reactive MD steps are necessary to initiate the 80 growing chains. This amounts to roughly 0.02% of the complete polymerization time t_∞. When choosing a capture radius of 0.40 nm for the initiation, 1174 reactive time steps are required for the initiation of the 80 growing chains. Here, the completion of the starting process covers 2% of t_∞. The slow propagation rate in both systems attenuates any difference in the initiation. In the case of $r_I = r_P = 0.40$ nm, the coupled initiation and propagation steps do not prevent the latest chains initiated from finding free monomers. For $r_I > r_P$ the 80 growing chains that were started already within 0.02% of the reaction will grow uniformly. The discussion in this last subsection has shown that the present RMD results are in line with basic principles of reaction (polymerization) kinetics. It is the slowest step of a process that determines the final product profile.[37] This is impressively seen in the bottom diagram of Figure 16. Here we have plotted the probability function $P(N_L)$ now derived for a polymerization where the formation of the I−P* is slower than the chain propagation. The RMD calculation leads to an extremely broad profile. Polymer chains containing more than 150 monomers are formed in this simulation. The small initiation radius $r_I = 0.40$ nm leads to an increase in the time required for all initiators to bind a monomer. Thus, the initiation step is extended over a long period. At the same time, the large propagation value $r_P = 0.55$ nm guarantees a fast chain growth whenever a I−P* unit has been formed. Therefore, a large number of monomers are connected by the first growing chains while few remain for the growth of the latest chains formed.

D. Comparison with Experiments and Analytical Results. In the discussion of the RMD results of polydisperse samples, we have emphasized that the tuning parameters r_I, r_P, and τ_r have a sizable influence on the molecular weight distribution $P(N_L)$, its mean value $\langle N_L \rangle_{sim}$, and the polydispersity index I_{Psim}. In this section, we relate the RMD-based quantities to simple analytical expressions (N_{La}, I_{Pa}) that are valid for a living/controlled polymerization as well as to experimental trends. We will show that the absence of termination reactions is only one condition for a living/controlled polymerization. The proximity to the limit of a living/controlled process is also determined by the absolute and relative speed for initiation and chain propagation; see below. If the initiation step is slow relative to the propagation, we will always have a deficit of I* leading to the formation of long chains (large polydispersity indices). This has been confirmed experimentally.[50−52] We next consider the overall speed of the polymerization under the assumption that the initiation and propagation steps require approximately the same time. In this case, the polydispersity increases with the speed. This has been observed experimentally in an atom transfer radical polymerization (ATRP) of styrene, whose reaction speed was modulated by using different iron halide complexes as catalysts.[52] For the fastest reactions, I_P values between 1.4 and 1.3 have been measured. A slight reduction of the speed has lowered I_P to 1.3, while a slow polymerization has been accompanied by a further decrease of I_P to 1.2. Conversions of 60 and 80% were reached in this ATRP study.

Let us continue with analytical formulas that are employed in experiments to discuss the living/controlled character of a polymerization process.[50−52] For a well-controlled polymerization (i.e., a process that yields narrow polymer size distribution), the expected average degree of polymerization N_{La} and polydispersity index I_{Pa} can be determined[38,52] theoretically by the ratio between the monomers that have reacted (ΔM) at a given time and the number of initiators N_I. For a conversion of 100% in our RMD simulations, $\Delta M = N_M - N_I$ is the number of monomers at the beginning of the reaction. We have

$$N_{La} = \frac{\Delta M}{N_I} \tag{5}$$

and

$$I_{Pa} = 1 + \frac{1}{N_{La}} - \frac{1}{(N_{La})^2} \quad (6)$$

The computational conditions adopted for the polydisperse samples imply $N_{La} = 3920/80 = 49$ and $I_{Pa} = 1.02$ ($D_P = 100\%$).

On the basis of the given experimental information and the analytical expressions (5) and (6), let us reconsider the RMD results derived for polydisperse samples. First, we want to highlight some peculiarities of the simulations with the help of figures. In one RMD run starting from a localized initiator distribution ($r = 0.55$ nm, $\tau_r = 5 \times 10^{-4}$ ns), we have modeled an extremely inefficient condition for a controlled polymerization (see top diagram in Figure 14). The small number of I* accessible at the beginning of the reaction strongly restricts the number of growing polymer chains. The outcome of such a condition is the formation of broad $P(N_L)$ profiles. In our special case, a distribution with two maxima has been observed. The first one has been found at a N_L value of roughly 10, and the second one at $N_L \approx 70$. But also in connection with a random distribution of the I*, a very broad $P(N_L)$ profile has been detected (see bottom diagram in Figure 16). Prerequisite for this curve shape is again an initiation step that is slow in comparison to the propagation. In our RMD simulations, it had been generated by capture radii fulfilling $r_I < r_P$. Already the results in Figures 14 and 16 have indicated that the RMD approach is able to reproduce general experimental trends of living polymerization reactions. Inefficient starting reactions imply broad $P(N_L)$ profiles (large I_P numbers). In the present approach, two mechanisms forcing such a polymerization process have been suggested: (i) inefficient starting reaction (here modeled by $r_I < r_P$) and (ii) localized starting configuration of the initiators which implies that many of the I* are in the inner region of the initiator droplet.

We continue our discussion with the RMD data in table 3. It summarizes $\langle N_L \rangle_{sim}$ and I_{Psim} (eqs 2 and 3) values that have been derived from single simulations under different conditions.

Case studies 1, 2, 3, and 4 are close to the boundary of a living/controlled polymerization. Nevertheless, examples 1 and 3 show that an enhanced velocity ($r = 0.55$ nm in 1 relative to $r = 0.40$ nm in 3) implies a larger deviation from $I_{Pa} = 1.02$ (i.e., 1.06 versus 1.016). In example 4, we are again closer to 1.02 due to the small $r_P = 0.40$ nm. The largest deviation from this limit is observed for example 5, where the slow starting reaction ($r_I = 0.40$ nm) compared to the propagation ($r_P = 0.55$ nm) leads to $\langle N_L \rangle_{sim} = 58.65$ and $I_{Psim} = 1.47$. In contrast to the case study of the previous subsection, which led to a bimodal $P(N_L)$ curve, a random distribution of the I* has been adopted in example 5.

The results of the present section can be summarized as follows. (1) The correlation of the RMD data with limiting values derived analytically for a living/controlled polymerization has shown that we are able to reproduce this limit by properly designed tuning parameters. (2) The RMD approach reproduces a general experimental trend, i.e., the increase of the polydispersity index for slow initiation and for high propagation speed. (3) It seems to be an advantage of the RMD simulations in the range of nanoseconds that they reproduce experimental trends derived for reaction times in the range of minutes. The present findings let us hope that the simulations on polydisperse samples go beyond a bare case study. In analogy to the RMD data derived for monodisperse samples, also the quantities calculated for polydisperse ones offer insight into experimental control parameters of a living polymerization.

TABLE 3: Simulated Average Degree of Polymerization $\langle N_L \rangle_{sim}$ and Polydispersity Index I_{Psim} for RMD Simulations under Different Conditions[a]

example	reactive conditions	$\langle N_L \rangle_{sim}$	I_{Psim}
1	$r_I = r_P = 0.55$, $\tau_r = 5 \times 10^{-4}$	49.99	1.06
2	$r_I = r_P = 0.55$, $\tau_r = 1 \times 10^{-2}$	49.99	1.015
3	$r_I = r_P = 0.40$, $\tau_r = 5 \times 10^{-4}$	50.79	1.016
4	$r_I = 0.55$, $r_P = 0.40$, $\tau_r = 5 \times 10^{-4}$	50	1.026
5	$r_I = 0.40$, $r_P = 0.55$, $\tau_r = 5 \times 10^{-4}$	58.65	1.47

[a] The quantities are derived for a conversion $D_P = 100\%$. They are compared with $N_{La} = 49$ and $I_{Pa} = 1.02$ (eqs 5 and 6). All simulations considered in this table are based on a random distribution of the initiators. The delay time τ_r is given in ns and r in nm.

6. Conclusions

In the present contribution, we have introduced a reactive MD approach equipped with a material-specific CG potential. We have chosen the polymerization of styrene monomers (represented by ethylbenzene) to polystyrene as a model. To simulate a living polymerization, irreversible bond formation and the absence of chain termination reactions have been assumed. For the mapping of the CG beads, we have employed a potential optimized on the basis of atomistic equilibrium MD simulations. It is characterized by system-specific radial and angle terms that are less straightforward to implement than generic potentials. The different degrees of sophistication in the potential are perhaps the strongest discriminator between recent generic models and the present implementation.

The RMD scheme developed requires the introduction of two input parameters. The first is the delay time τ_r between two reactive MD steps, which is characteristic for simulation methods of the MD or MC type. The second parameter is related to an activation term for bond formation. The activation energy for this process is indirectly determined by so-called capture radii r_I and r_P defining the possibility that two nonbonded monomers form a chemical bond in a reactive step. This process is implemented as the transition from a nonbonded to a bonded CG potential. In our first numerical study, we have allowed an instantaneous transition from a nonbonded to a bonded potential in a reactive process. The simulations discussed in the third section have verified that there is no heat up in the sample that exceeds the fluctuations in conventional equilibrium simulations. The largest T enhancement found in the case of fast reaction dynamics is still too small to be significant.

The capability of the present RMD formalism has been validated for monodisperse samples. The reactive MD code reproduces the results of equilibrium simulations. Densities, end-to-end distances, and radii of gyration as well as different geometrical distribution functions have been chosen for the comparison of RMD and MD results. In this part of our work, we have shown that the present RMD approach offers a straightforward access to equilibrated polymer configurations, which is an additional application for it. Previous coarse-grained RMD studies were more oriented in generating equilibrated polymer structures. Thus, the natural possibility to track the polymerization dynamics by RMD simulations had not been fully explored. Despite all simplifications, the present model has been successful in reproducing the basic characteristics of living polymerization. The results derived for polydisperse samples have also been correlated favorably to experimental trends. The different case studies clearly emphasized the power of future RMD studies for (living) polymerizations.

Acknowledgment. The present work has been supported generously by the DFG priority program SPP1369. We are highly grateful to Dr. H.-J. Qian who has provided the ethylbenzene and polystyrene coarse-grained potentials presently used. Fruitful discussions with our Alexander-von-Humboldt guest scientist Prof. Xuehao He (Tianjin University, China) are also gratefully acknowledged. Finally, we want to thank Drs. Thomas Müller and Frédéric Leroy for their continuous support in the initial phase of the present research.

References and Notes

(1) Leung, Y. K.; Eichinger, B. E. *J. Chem. Phys.* **1984**, *32*, 3877.
(2) Faulon, J. L. *J. Comput. Chem.* **2001**, *22*, 580.
(3) Alperstein, D.; Dodiuk, H.; Kenig, S. *Acta Polym.* **1998**, *49*, 594.
(4) Zhang, Z.; Yamashita, T.; Wong, C. P. *Macromol. Chem. Phys.* **2005**, *206*, 869.
(5) Cheng, K.-C.; Don, T.-M.; Rwei, S. P.; Li, Y.-C.; Duann, Y.-F. *J. Polym. Sci., Part B: Polym. Phys.* **2002**, *40*, 1857.
(6) Wen, M.; Scriven, L. E.; McCormick, A. V. *Macromolecules* **2003**, *36*, 4140.
(7) Gupta, S.; Westermann-Clark, G. B.; Bitsanis, I. *J. Chem. Phys.* **1993**, *98*, 634.
(8) Milchev, A.; Wittmer, J. P.; Landau, D. P. *J. Chem. Phys.* **2000**, *112*, 1606.
(9) Khare, K.; Paulaitis, M.; Lustig, S. R. *Macromolecules* **1993**, *26*, 7203.
(10) Gao, J. *J. Chem. Phys.* **1995**, *102*, 1074.
(11) Akkermans, R. L. C.; Toxvaerd, S.; Briels, W. J. *J. Chem. Phys.* **1998**, *109*, 2929.
(12) Toxvaerd, S. *J. Mol. Liq.* **2000**, *84*, 99.
(13) Svaneborg, C.; Grest, G. C.; Everaers, R. *Polymer* **2005**, *46*, 4283.
(14) Berardi, R.; Micheletti, D.; Muccioli, L.; Ricci, M.; Zannoni, C. *J. Chem. Phys.* **2004**, *121*, 9123.
(15) Mavrantzas, V. G.; Boone, T. D.; Zervopoulo, E.; Theodorou, D. N. *Macromolecules* **1999**, *32*, 5072.
(16) Auhl, R.; Everaers, R.; Grest, G. S.; Kremer, K.; Plimpton, S. J. *J. Chem. Phys.* **2003**, *119*, 2718.
(17) Pant, P. V. K.; Theodorou, D. N. *Macromolecules* **1995**, *28*, 7224.
(18) Karayiannis, N. C.; Mavrantzas, V. G.; Theodorou, D. N. *Phys. Rev. Lett.* **2002**, *88*, 105503.
(19) Liu, H.; Qian, H.-J.; Zhao, Y.; Lu, Z.-Y. *J. Chem. Phys.* **2007**, *127*, 144903.
(20) Corezzi, S.; De Michele, C.; Zaccarelli, E.; Fioretto, D.; Sciortino, F. *Soft Matter* **2008**, *4*, 1173.
(21) Perez, M.; Lame, O.; Leonforte, F.; Barrat, J.-L. *J. Chem. Phys.* **2008**, *128*, 234904.
(22) Sciortino, F.; De Michele, C.; Douglas, J. F.; Tartaglia, P. *J. Chem. Phys.* **2007**, *126*, 194903.
(23) Sciortino, F.; De Michele, C.; Douglas, J. F. *J. Phys.: Condens. Matter* **2008**, *20*, 155101.
(24) Xu, J.; Kjelstrup, S.; Bedeaux, D. *Phys. Chem. Chem. Phys.* **2006**, *8*, 2017.
(25) Smith, K. D.; Stoliarov, S. I.; Nyden, M. R.; Westmoreland, P. R. *Mol. Simul.* **2007**, *33*, 361.
(26) Jiang, B.; Selvan, M. E.; Keffer, D. J.; Edwards, B. J. *J. Phys. Chem. B* **2009**, *113*, 13670.
(27) Nyden, M. R.; Stolianov, S. I.; Westmoreland, P. R.; Guo, T. X.; Jee, C. *Nat. Sci. Eng. A* **2004**, *365*, 114.
(28) van Duin, A. C. T.; Dasgupta, S.; Lorant, F.; Goddard III, W. A. *J. Phys. Chem. A* **2001**, *105*, 9396.
(29) van Duin, A. C. T.; Strachan, A.; Stewman, S.; Zhang, Q.; Xu, X.; Goddard III, W. A. *J. Phys. Chem. A* **2007**, *107*, 3803.
(30) Turner, H. C.; Brennan, J. K.; Lísal, M.; Smith, W. R.; Johnson, J. K.; Gubbins, K. E. *Mol. Simul.* **2008**, *34*, 119.
(31) Qian, H.-J.; Carbone, P.; Chen, X.; Karimi-Varzaneh, H. A.; Liew, C. C.; Müller-Plathe, F. *Macromolecules* **2008**, *24*, 9919.
(32) Rossinsky, E.; Müller-Plathe, F. *J. Chem. Phys.* **2009**, *130*, 134905.
(33) Algaer, E.; Alaghemandi, M.; Böhm, M. C.; Müller-Plathe, F. *J. Phys. Chem. A* **2009**, *113*, 11487.
(34) Algaer, E.; Alaghemandi, M.; Böhm, M. C.; Müller-Plathe, F. *J. Phys. Chem. B* **2009**, *113*, 14596.
(35) Theoretical Physical Chemistry, TU-Darmstadt, Home Page: http://www.theo.chemie.tu-darmstadt.de.
(36) Szwak, M.; van Beylen, M. *Ionic Polymerization Living Polymers*; Chapman and Hall: New York, 1993.
(37) Allen, P. E. M.; Patrick, C. R. *Kinetics and Mechanism of Polymerization Reactions*; Ellis Horwood: Chichester, UK, 1974.
(38) Rubinstein, M.; Colby, R. H. *Polymer Physics*; Oxford University Press: Oxford, UK, 2006.
(39) Reith, D.; Pütz, M.; Müller-Plathe, F. *J. Comput. Chem.* **2003**, *24*, 1624.
(40) Binder, K.; Stauffer, D. *Application of the Monte Carlo Method in Statistical Physics*; Springer Verlag: Berlin, 1987.
(41) Böhm, M. C.; Elsässer, C.; Fähnle, M.; Brandt, E. H. *Chem. Phys.* **1989**, *130*, 65.
(42) Sujita, Y.; Okamoto, Y. *Chem. Phys. Lett.* **1999**, *314*, 141.
(43) Dollin, M.; Szkuhran, A. R.; Georges, M. K. *J. Polym. Sci., Part A: Polym. Chem.* **2007**, *45*, 5487.
(44) Miura, Y.; Mibae, S.; Moto, H.; Nakamura, N.; Yamada, B. *Polym. Bull.* **1999**, *42*, 17.
(45) Berendsen, H. J. C.; Postma, P. M.; van Gunsteren, W. F.; Di Nola, A.; Haak, J. R. *J. Chem. Phys.* **1984**, *81*, 3684.
(46) Höcker, H.; Blake, G. J.; Flory, P. J. *Trans. Faraday Soc.* **1971**, *67*, 2251.
(47) Des Cloiseaux, J.; Jannink, G. *Polymers in Solution; Their Modelling and Structure*; Clarendon: Oxford, UK, 1990.
(48) Sun, Q.; Faller, R. *Macromolecules* **2006**, *39*, 812.
(49) Fox, T. G.; Flory, P. J. *J. Appl. Phys.* **1950**, *21*, 581.
(50) Matyjaszewski, K. In *controlled Radical Polymerization*; ACS Symposium Series; American Chemical Society: Washington, DC, 1998; Chapter 1.
(51) Matyjaszewski, K.; Wang, J. L.; Grimaud, T.; Devon, A. S. *Macromolecules* **1998**, *31*, 1527.
(52) Matyjaszewski, K.; Mingli, W.; Xia, J.; McDermott, N. E. *Macromolecules* **1997**, *30*, 8161.

JP107001E